Positive–negative birefraction phenomenon for TM polarization in annular photonic crystal

Yuan Zhang (张 园)[1], Yifeng Shen (沈义峰)[1,2*], Jie Zhou (周 杰)[1], Yongchun Wang (王永春)[1], Fangfang Wu (吴芳芳)[1], Jian Sun (孙 建)[1], and Changqing Guo (郭昌清)[1]

[1]*Physics Department of the Science College, China University of Mining and Technology, Xuzhou 221116, China*

[2]*Surface Physics Laboratory, Fudan University, Shanghai 200433, China*

[*]*Corresponding author: shen_syf@163.com*

Received August 18, 2010; accepted October 28, 2010; posted online January 28, 2011

We propose a two-dimensional (2D) annular photonic crystal (APC) with dual equi-frequency contours (EFCs) in one band. The refractive behaviors of a Gaussian beam incident from air to the APC are analyzed by the EFC analysis and finite-difference time-domain (FDTD) method. The results show the positive-negative birefraction phenomenon for the transverse magnetic (TM) polarization in the same band occurs at the interface between air and the APC, and the surface termination of the APC has a large effect on the strength of the negatively refracted beam.

OCIS codes: 260.1180, 350.4238, 350.3618, 350.7420.

doi: 10.3788/COL201109.022601.

Photonic crystal (PC) is an artificial periodic dielectric structure, which exhibits many specific properties such as photonic band gap, self-collimation and superprism effects, and negative refraction[1−6]. Negative refraction is a very interesting phenomenon, wherein the refracted and incident beams stay on the same side of the normal. Veselago initially predicted the negative refraction to be occurring at the interface between an ordinary homogenous dielectric and one conceptual material with simultaneous negative values of dielectric permittivity and magnetic permeability[7]. However, the negative refraction in PCs can occur even without a negative refractive index[8]. Moreover, positive and negative refractions can even occur simultaneously in PCs[9−15]. There are three main cases for this phenomenon. The first one is due to high-order diffractions[9−11]. The zero-order and high-order (–1 or +1) diffractions are satisfied simultaneously due to the surface periodic diffraction. The second is due to the incident beam having different wave vectors because of narrow beam width[12]. The different wave vectors may induce both positive and negative refractions. However, these two cases are not rigid birefraction phenomena for one polarization state. The last case is the birefraction phenomenon due to the overlapping of different bands[13−15]. At the overlapping band region, the PC has two equi-frequency contours (EFCs) corresponding to different bands. Each EFC yields one refracted beam. To our knowledge, no one has demonstrated the birefraction phenomenon for one polarization in the same band. This means that PCs should have dual EFCs at one frequency in the same band, which may be very difficult for standard PCs. Annual photonic crystals (APCs) have recently attracted much attention due to more adjustable parameters. Many promising properties have been found in APCs[16−19]. In this letter, we propose a two-dimensional (2D) square lattice APC, which can exhibit dual EFCs in the same band, and study the refractive behaviors of a Gaussian beam incident from air to the APC through EFC analysis and the finite-difference time-domain (FDTD) method. The positive-negative birefraction phenomenon in the same band is initially demonstrated by the FDTD simulations.

The system we consider is a 2D APC, which is a square

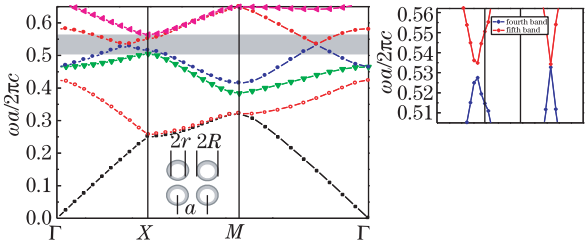

Fig. 1. Band structure of the APC, with the inset showing the APC structure. R and r are the outer and inner ring radii of the ring-shaped-pillar, respectively, with $R = 0.45a$ and $r = 0.35a$. The grey region indicates the considering bands, while the figure at the top right corner is the partial enlarged drawing of the corresponding grey region.

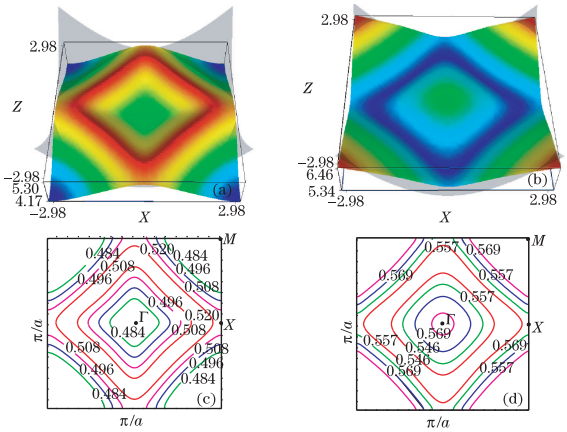

Fig. 2. Band surfaces of (a) the fourth band and (b) the fifth band; EFCs of (c) the fourth band and (d) the fifth band . Γ, X, and M are the corresponding symmetric points of the first Brillion zone.

lattice with ring-shaped pillar. Both the background and the low dielectric cores are air, while the ring-shaped pillar is a high dielectric with a refractive index of $n = 3.4$. The inner ring radius r and the outer ring radius R are $0.35a$ and $0.45a$, respectively, where a is the lattice constant. This APC has a peculiar band structure for transverse magnetic (TM) polarization (the electric field **E** is parallel to the axis of the ring-shaped pillar), as shown in Fig. 1. The band structure is calculated by the plane wave expansion (PWE) method[20]. We focus on the fourth and fifth bands (the grey region), which interact with each other and lead to a complete mini band gap at the frequency of $\omega = 0.534(2\pi c/a)$, where c is the speed of light in vacuum. Each of these bands has both a positive band slope part and a negative band slope part, indicating that they have two modes with different simultaneous behaviors. One is right handed ($\mathbf{v}_g \cdot \mathbf{k} > 0$, where $\mathbf{v}_g$ and $\mathbf{k}$ are the group velocity and the wave vector, respectively), while the other is left handed ($\mathbf{v}_g \cdot \mathbf{k} < 0$).

To have more details of these two bands, we also calculate the band surfaces and the EFCs. Figures 2(a) and (b) show the band surfaces of the fourth and fifth bands, respectively. Figures 2(c) and (d) show the corresponding EFCs.

As can be seen from Fig. 2(a), the fourth band surface in the first Brillion zone is like a volcanic vent with a square shape. The center and the four corners are concave. Figure 2(b) shows that the fifth band surface has an opposite curvature: both the center and the corners are convex. Thus, unlike ordinary PCs, there are two EFC curves at one frequency for our APC in each band, as shown in Figs. 2(c) and (d). The frequency range is from $0.48(2\pi c/a)$ to $0.52(2\pi c/a)$ for the fourth band and from $0.54(2\pi c/a)$ to $0.58(2\pi c/a)$ for the fifth band. As an example, we choose the frequency $\omega = 0.546(2\pi c/a)$, as shown in Fig. 2(d). The dual EFC curves are both roughly square shaped rotated by 45° and centered at the Γ point, implying a self-collimation effect along the Γ-M direction in the PC. Moreover, the inner EFC shrinks, whereas the outer EFC expands with the increase in frequency. Because the direction of the group velocity is perpendicular to the EFC and points to the EFC with a higher frequency, the group velocity is inward and almost antiparallel to the wave vector for the inner EFC. This is a left-handed behavior for the inner EFC, whereas it is a right-handed behavior for the outer EFC. Meanwhile, this is an inverse case for the fourth band (in Fig. 2(c)). The inner one corresponds to the right-handed behavior, whereas the outer one is the left-handed behavior. Thus, this APC has a rather peculiar character. Thus, it can be the case that it is a right-handed material for one mode but a left-handed material for the other mode.

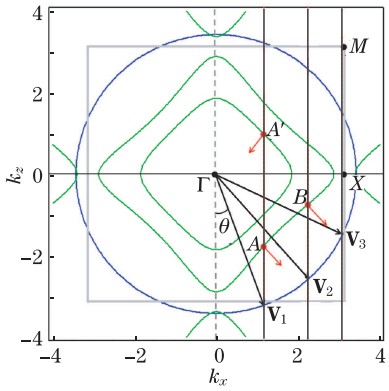

Fig. 3. EFC analysis for a incident wave with different angles θ of 25°, 40°, and 65°. The grey square represents the first Brillion zone; the horizontal line indicates the interface; the vertical dashed line refers to the normal of the interface. The circle is the EFC of air; the curves with roughly square shapes are the EFCs of the APC; the three vertical lines are the **k**-conservation lines. The long arrows indicate the incident wave vector with different angles; the short arrows indicate the group velocities of refracted beams in the APC.

Since the APC has dual EFCs with different behaviors at the self-collimation effect region, different phenomena may be found in this system. We investigate the reflection and refraction of a Gaussian beam at the interface between a homogeneous medium and the APC. We consider the homogeneous medium to be air and the surface termination to be along the Γ-X direction, and

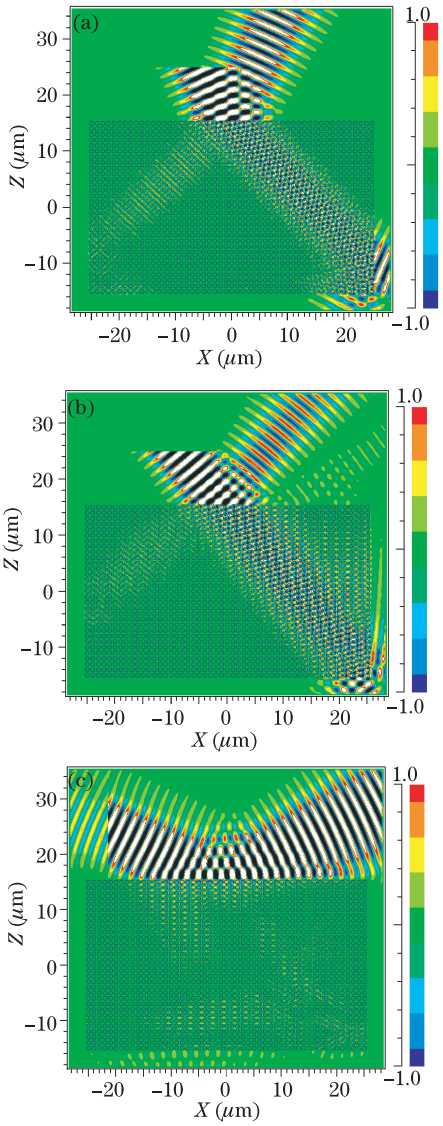

Fig. 4. Electric field contour with different incident angles for the complete APC without surface termination simulated by the FDTD method. (a) $\theta = 25°$; (b) $\theta = 40°$; (c) $\theta = 65°$.

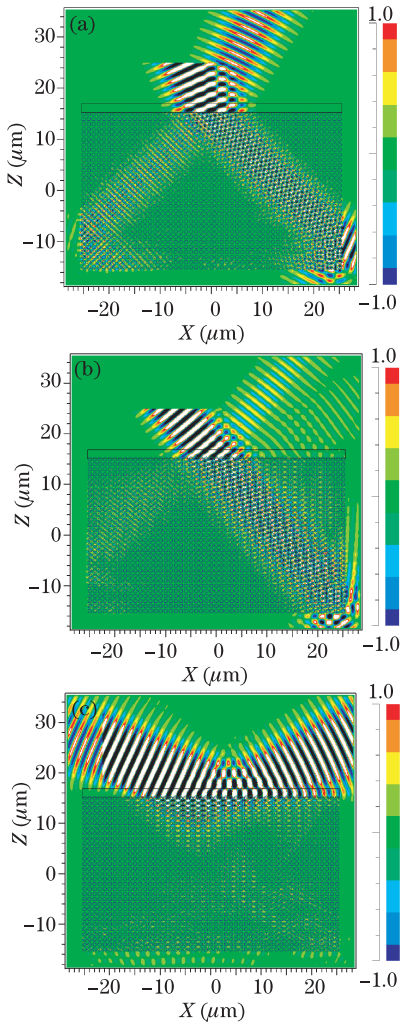

Fig. 5. Electric field contour with different incident angles for APC with an optimum surface termination simulated by the FDTD method. (a) $\theta = 25°$, $d = 0.17a$; (b) $\theta = 40°$, $d = 0.40a$; (c) $\theta = 65°$, $d = 0.40a$.

an EFC analysis is done. For convenience, we expand the **k** domain out of the first Brillion zone. The working frequency is chosen to be $\omega = 0.546(2\pi c/a)$ in the fifth band.

Figure 3 shows the EFCs of the APC and the EFC of air at the working frequency. The EFC of air has entered the second Brillion zone and is larger than the dual EFCs of the APC in the first Brillion zone. There are two requirements to ascertain the direction of the refracted beam. The refracted beam and the incident beam should have the same frequency and the same transmission direction along the vertical direction. The wave vector of the refracted beam should obey the **k**-conservation relation: $\mathbf{k}_{//}^{\mathrm{inc}} = \mathbf{k}_{//}^{\mathrm{ref}} + \mathbf{G}_{//}$, where $\mathbf{k}_{//}^{\mathrm{inc}}$ and $\mathbf{k}_{//}^{\mathrm{ref}}$ are the wave vector components parallel to the interface for the incident and refracted beams, respectively, and $\mathbf{G}_{//}$ is the parallel component of any reciprocal lattice vector. The different incident angles would then induce different refracted beams. We can divide the whole case into three utilizing simple geometrical analyses if the incident angle is $\theta < 32.8°$, and the **k**-conservation line (vertical line) and the EFCs of the APC will intersect at both points A' and A. Therefore, there are two refracted beams for this case: negative and positive. This corresponds to the birefraction phenomenon. If the incident angle is $32.8° < \theta < 59.8°$, the **k**-conservation line and the outer EFC of the APC only intersect at point B, thus there is only one positive refracted beam. If $59.8° < \theta$, the **k**-conservation line drops into a partial gap and does not cross any EFCs of the PC, thus there is no refracted beam; this corresponds to a total internal reflection.

Since only a single wave vector is considered, the above analysis is valid only for a plane wave. However, in experiments and real applications, a Gaussian beam is usually used, rather than a plane wave. A Gaussian beam with a finite spatial width can be regarded as a series of plane waves with different wave vectors in the **k** space. These different wave vectors strongly depend on the spatial width of the Gaussian beam[12]. The wider the spatial width is, the smaller the corresponding region in the **k** space is. Hence, in the following FDTD simulations, the waist width of the Gaussian beam is fixed at $12a$, which is approximately large enough for the Gaussian beam to be regarded as a plane wave (much larger than $4a$ in Ref. [12]). In the simulations, we consider an APC sample with a size of $50a\times$ $30a$. The air-PC interface is along the Γ-X direction. We use the Berenger's perfectly matched layer (PML) absorbing boundary conditions[21]. Each unit cell consists of 64 × 64 Yee cells. Thus, the spatial intervals are $\Delta_x = a/64$ and the time increments are $\Delta_t = \Delta_x/2c$. The Gaussian beam is TM polarized.

We consider a complete APC, which implies that the PC has a row of intact ring-shaped pillars at the air-PC boundary. Figure 4 shows the field distributions of the Gaussian beam that is incident to the PC from air at different angles. For Fig. 4(b), the incident angle is 40° and only one positive refracted beam exists in the PC, which agrees well with the analysis of the second case in Fig. 3. For Fig. 4(c), the incident angle is 60° and the electric field is hardly penetrating into the PC, which implies the total internal reflection as shown in the third case in Fig. 3. The reflection at the reverse direction of the incident beam is the higher-order reflection beam (–1 order). However, for Fig. 4(a), the FDTD simulation result seems not in agreement with the analysis of the first case in Fig. 3. The EFC analysis indicates that there is a birefraction phenomenon for the incident angle of $\theta = 25°$; however, the simulation result only gives a positive refracted beam. If the left part of the PC is examined more carefully, a very weak light beam propagating along the negative direction can be found, as point A' indicated in Fig. 3. Therefore, the Bloch mode with a left-handed behavior is much weaker than the one with a right-handed behavior, implying that the inner Bloch mode of the dual EFCs is hardly activated in a complete APC for an incident field from air. To demonstrate the negative-positive birefraction clearly, the intensity of the Bloch mode related to the inner EFC should be improved.

To determine the effect of surface termination to the activation of Bloch modes, we define the surface termination d= 0 as the case wherein the PC has a row of intact ring-shaped pillars at the air-PC boundary. This means that the interface between the air and the PC is only at the upper edge of the top row of ring-shaped pillars. In addition, for $d > 0$ for example d= $0.2a$ means

that the interface is moved along the negative z direction with a movement of $0.2a$ and cuts into the PC system. In the FDTD simulation, we cover the PC system with an air slab (the rectangular area at the top surface of the PC), and the overlapping regions of the top row of ring-shaped pillars are removed in the actual calculations. Xiao *et al*. indicated that surface termination may enhance the transmission of light beam due to the excitation of surface waves[22,23]. Thus we can optimize the value of surface termination d to enhance the transmission of the refracted beams (we consider to reduce the reflection at the interface in actual simulations) in the simulation process. The optimum parameters obtained are $d = 0.17a$, $0.40a$, and $0.40a$ for the incident angles $\theta = 25°$, $40°$, and $65°$, respectively. The surface termination only modifies the coupling intensity between the incident field and the Bloch modes, but does not change the propagating directions of the refracted beams.

Figure 5 shows the field distributions of the Gaussian beam that is incident to the APC with corresponding optimum value of d at different angles. For $\theta = 25°$, there are two distinct refracted collimating beams: one is negatively refracted (corresponding to point A') and the other is positively refracted (corresponding to point A). This is the positive-negative birefraction at only one band for TM polarization and agrees relatively well with the prediction of the EFC analysis in Fig. 3. In addition, this simulation result also shows that surface coupling is very important for the excitation of the Bloch mode. For $\theta = 40°$, there is only one positively refracted beam, and the reflection is greatly depressed. For $\theta = 65°$, although the incident field can permeate into the PC with a depth of several layers, there is still no refracted beam and all energy is totally reflected, corresponding to a total internal reflection behavior. The high-order reflection beam (-1 order), which propagates along the direction antiparallel to the incident direction, is greatly enhanced. Hence, the surface termination can adjust the energy disposal among different modes.

In conclusion, we investigate the refraction behaviors of a Gaussian beam incident from the air to the APC with dual EFCs and demonstrate the negative-positive birefraction at the same band in our APC system. FDTD simulation results agree well with the theoretical EFC analysis. We also compare the cases of zero surface termination d=0 with the cases of different optimum surface terminations and conclude that appropriate surface termination is important to excite specific Bloch mode.

This work was supported by the Science Foundation of China University of Mining and Technology (No. OK061065) and the Fundamental Research Funds for the Central Universities (No. 2010LKWL10).

References

1. E. Yablonovitch, Phys. Rev. Lett. **58,** 2059 (1987).
2. S. John, Phys. Rev. Lett. **58,** 2486 (1987).
3. H. Kosaka, T. Kawashima, A. Tomita, M. Notomi, T. Tamamura, T. Sato, and S. Kawakami, Phys. Rev. B **58,** R10096 (1998).
4. H. Kosaka, T. Kawashima, A. Tomita, M. Notomi, T. Tamamura, T. Sato, and S. Kawakami, Appl. Phys. Lett. **74,** 1212 (1999).
5. M. Notomi, Phys. Rev. B **62,** 10696 (2000).
6. S. Feng, C. Ren, D. Xu, and Y. Wang, Chin. Opt. Lett. **7,** 849 (2009).
7. V.G. Veselago, Sov. Phys. Uspekhi **10,** 509 (1968).
8. C. Luo, S. G. Johnson, J. D. Joannopoulos, and J. B. Pendry, Phys. Rev. B **65,** R201104 (2002).
9. S. Foteinopoulou and C. M. Soukoulis, Phys. Rev. B **67,** 235107 (2003).
10. S. Foteinopoulou and C. M. Soukoulis, Phys. Rev. B **72,** 165112 (2005).
11. Y. Luo, W. Zhang, Y. Huang, J. Zhao, and J. Peng, Opt. Lett. **29,** 2920 (2004).
12. A. Kim, K. B. Chung, and J. W. Wu, Appl. Phys. Lett. **89,** 251120 (2006).
13. R. Gajic, R. Meisels, F. Kuchar, and K. Hingerl, Opt. Express **13,** 8596 (2005).
14. M. H. Lu, C. Zhang, L. Feng, J. Zhao, Y. F. Chen, Y. W. Mao, J. Zi, Y. Y. Zhu, S. N. Zhu, and N. B. Ming, Nature Material **6,** 744 (2007).
15. X. Kang, G. Li, and Y. Li, J. Opt. Soc. Am. B **26,** 60 (2009).
16. H. Kurt and D. S. Citrin, Opt. Express **13,** 10316 (2005).
17. H. Kurt, R. Hao, Y. Chen, J. Feng, J. Blair, D. P. Gaillot, C. Summers, D. B. Citrin, and Z. Zhou, Opt. Lett. **33,** 1614 (2008).
18. A. Cicek and B. Ulug, Opt. Express **17,** 18381 (2009).
19. J. Hou, D. S. Gao, H. M. Wu, and Z. P. Zhou, Opt. Comm. **282,** 3172 (2009).
20. J. D. Joannopoulos, R. D. Meade, and J. N. Winn, *Photonic Crystals* (Princeton, New York, 1995.)
21. A. Taflove, *Computational Electrodynamics* (Artech House, Boston, 1995.)
22. S. S. Xiao, M. Qiu, Z. C. Ruan, and S. L. He, Appl. Phys. Lett. **85,** 4269 (2004).
23. R. Moussa, T. Koschny, and C. M. Soukoulis, Phys. Rev. B **74,** 115111 (2006).